ISSN: 0067-2904

Analyzing Materials and Determining their Physical Properties Using Spectral Sensing Technology from Satellite Images: Methodology and Applications

Salema Sultan Salman [1*], Ban S. Ismael[2]
[1]*Clinical Laboratory Sciences, College of Pharmacy, University of Baghdad , Baghdad, Iraq*
[2] *Department of Astronomy and Space, College of Science, College, University of Baghdad , Baghdad, Iraq*

Received: 22/12/2024 Accepted: 28/3/2025 Published: 30/3/2026

Abstract

The spectral remote sensor technology was used to study the Kurdistan region of Iraq to determine the characteristics of surface minerals and by analyzing satellite images across multiple spectral ranges, distinctive spectral signatures were specified for several metals such as zinc (ZN), Lead (PB), and Parium (BA), as well as the use of thermal infrared to detect free abnormalities and the results were verified through field measurements and admonitory, where the selection accuracy was 85% according to the absolute error (MAPE) and 0.045 for RMSé and the results showed that spectral signatures for metals were distributed in nearby and remote IR ranges, helping to determine mineral sediments such as zinc and lead in carbonate rocks and infrared data and it also revealed a surface temperature between 20°C and 35°C, with thermal anomaly indicating metal concentrations and the study confirms the effectiveness of spectral remote sensing as an inexpensive and accurate tool for minerals, which enhances sustainable resource management strategies in Iraq.

Keywords: Spectral remote sensing, mineral exploration, thermal infrared (TIR), geophysical properties.

تحليل المواد وتحديد خصائصها الفيزيائية باستخدام تقنية الاستشعار الطيفية من صور الأقمار الصناعية: المنهجية والتطبيقات

سليمة سلطان سلمان [1]*, بان صباح اسماعيل [2]
[1]فرع العلوم المختبرية السريرية , الصيدلة , بغداد , بغداد , العراق
[2] قسم الفلك والفضاء, العلوم , بغداد , بغداد , العراق

الخلاصة

تم استخدام تقنية المستشعرات عن بُعد الطيفية لدراسة منطقة كردستان في العراق لتحديد خصائص المعادن السطحية وتحليل صور الأقمار الصناعية عبر نطاقات طيفية متعددة ، تم تحديد توقيعات طيفية مميزة للعديد من المعادن مثل الزنك (Zn) ، الرصاص (Parium (BA)،PB) ، وكذلك استخدام الأشعة تحت الحمراء الحرارية للكشف عن تشوهات حرة تم التحقق من النتائج من خلال القياسات الميدانية و

* Email: sultan@copharm.uobaghdad.edu.iq

edesontry ، حيث كانت دقة الاختيار 85 ٪ وفقًا للخطأ المطلق (MAPE) و 0.045 لـ RMSé و RMS. أظهرت النتائج أن التوقيعات الطيفية للمعادن قد تم توزيعها في نطاقات الأشعة تحت الحمراء القريبة والبعيدة ، مما يساعد على تحديد الرواسب المعدنية مثل الزنك والرصاص في صخور الكربونات وبيانات الأشعة تحت الحمراء عن درجة حرارة السطح بين 20 درجة مئوية و 35 درجة مئوية ، مع شذوذ حراري تشير إلى تركيزات المعادن والدراسة تؤكد فعالية الاستشعار عن بُعد الطيفي كأداة غير مكلفة ودقيقة للمعادن ، مما يعزز استراتيجيات إدارة الموارد المستدامة في العراق..

1-Introduction

Spectral remote sensing technology is one of the most advanced applications, as it relies on analyzing electromagnetic radiation reflected or emitted by materials to understand their physical and chemical properties with high accuracy [1]. This technology is based on the fundamental physical principles of light and electromagnetic radiation, utilizing the entire electromagnetic spectrum, including wavelengths from ultraviolet to infrared and microwave [2], and the interaction between radiation and matter is influenced by a range of physical phenomena such as reflection, absorption, emission, and refraction, making each material's spectral signature unique and capable of revealing its chemical and structural properties [3].

Spectral remote sensing begins with data collection using satellite-borne sensors such as Landsat, MODIS, and Sentinel. These sensors record electromagnetic radiation across multiple spectral bands (multispectral and hyperspectral), with each band providing precise information related to the properties of the target materials, such as atomic and molecular structure [4]. These models represent the basis for understanding how radiation interacts with matter and physical laws, like Planck's law of thermal radiation, which describes radiation distribution based on temperature, and the laws of reflection and refraction, which explain how radiation interacts with different surfaces [5].

Data accuracy depends on processing the raw images generated by the sensors using advanced techniques to improve their quality and remove noise caused by factors like the atmosphere or sensor sensitivity , selek [4] proposed the use of "2D histogram equalization" for contrast enhancement, while Li et al. [11] suggested a method based on dominant brightness level analysis and adaptive intensity transformation for hyperspectral image enhancement and these processes aim to enhance images for analyzing the physical properties of materials and in the analysis phase, advanced mathematical and physical models are applied to understand how radiation interacts with matter, where spectral patterns resulting from different materials are studied based on the interaction between atomic particles and radiation [6] , Additionally, models are used to analyze complex physical phenomena such as interference and diffraction in crystalline materials [7] and these models allow for the extraction of accurate information about materials' internal composition and physical and chemical properties [8].

Spectral remote sensing technology is applied across various fields, such as natural resource exploration, environmental monitoring, and water resource management [10] , for instance, researchers have used this technology to monitor temporal changes in land use and their impact on surface temperatures and this demonstrates the technology's potential to study the relationships between human activities and the environment and the results are carefully compared with laboratory measurements using techniques like X-ray spectroscopy or electron microscopy to ensure the accuracy of the models and the accuracy of the results is evaluated using criteria such as Root Mean Square Error (RMSE) or Mean Absolute Percentage Error

(MAPE), ensuring the models align with physical reality as described in [6], Spectroscopic remote sensing technology is considered one of the most advanced physical tools for studying materials and analyzing their chemical and physical properties on a large scale and this technology is based on studying the physical interactions between electromagnetic radiation, Matter, where spectral responses are recorded across multiple electromagnetic spectrum bands, such as visible light, infrared rays, and ultraviolet rays, and these responses give accurate information about the nature of the material, its molecular structure, Its thermal and optical properties, and other physical properties, as spectral sensing technology relies on the laws of classical and quantum physics.

The theoretical basis is Planck's law of thermal radiation, which describes how materials emit energy based on their temperature, and Kirchhoff's law, which relates the absorptivity and emissivity of any material. Each material has a distinct spectral fingerprint that depends on its atomic composition and crystal structure [18]; Landsat retrieves multispectral data to analyze materials' thermal and optical properties. For example, Landsat data were used in a study [14] to estimate surface temperature and monitor land cover. At the same time, MODIS was relied upon to monitor large environmental phenomena; a study [9] used MODIS data to analyze water vapor and surface temperature, allowing an accurate assessment of ecological changes; sentinel provides hyperspectral information that helps identify chemical elements and minerals based on spectral interaction [3] and based on spectroscopic experiments, metals can be accurately determined using spectral fingerprints.

A study[8] combined radar and optical data to analyze geological regions, and the study showed that different metals show distinct reflectivity patterns due to the interaction of radiation with the crystal structure and the study[4] used spectroscopic models to analyze surface temperature and emissivity and thermal radiation emitted by soil and plants was measured using thermal sensors and this data was used to develop models linking thermal emission to the physical properties of materials and the study [11] focused on analyzing the relationship between changes in ground cover and surface temperature using spectral data [12] and the study revealed that areas with dense vegetation absorb more radiation, reducing the surface temperature , At the same time, arid regions show higher spectral reflectance, leading to a rise in temperature , spectral data requires improvements to reduce noise caused by the atmosphere or sensors , A study [13] used wavelet analysis to improve the contrast in spectral images, which helped detect fine details of materials via contrast techniques such as [14], which improved the accuracy of the data by adjusting the gradients , color, brightness, intersection, and their analysis[15] , using low- and high-frequency scaling [10] provides a way to understand spectral reflectances accurately, Physical models represent the cornerstone for analyzing spectral data through the thermal emission model, which focuses on studying the radiation emitted by thermal surfaces, and through the spectral dispersion model, which is used to understand how radiation propagates over irregular surfaces [16].

The evaluation is done through laboratory experiments by comparing the results with spectroscopic analysis [17] and the researchers seek to use X-ray spectroscopy, which is used to confirm spectral results obtained from satellites, and they compared the data [18]; it has been extracted from spectral sensing with laboratory experiments and found a high agreement proving the effectiveness of the models used [19-20] where criteria such as root mean square error (RMSE) are used to determine the accuracy of spectral models in comparing predictions with actual data as in [4-5] , spectroscopic remote sensing technology represents a tremendous physical advance in studying the properties of materials from a distance [21] , using accurate physical models and supporting laboratory experiments, this technology has

proven its feasibility in wide applications, including exploring natural resources, studying environmental changes, and analyzing the physical properties of materials [22]; with the development of digital sensors and processors, this technology will continue pushing scientific knowledge's boundaries toward more advanced applications.

3-Methodology

Due to its geological and environmental diversity, Iraq was chosen as the study area, and it is an ideal region for utilizing spectroscopic remote sensing techniques to analyze materials and determine their physical properties. This study uses satellite imagery to analyze the characteristics of Iraq's natural resources, land uses, and environmental dynamics. The methodology for analyzing materials using spectral remote sensing integrates satellite observations, laboratory experiments, and physical modeling to determine material properties such as emissivity, reflectivity, and thermal conductivity, and this multidisciplinary approach ensures precision and reliability by employing mathematical models, experimental techniques, and validation methods. This study adopts several key parameters and models for analysis, and below are the relevant equations for the most important parameters:

1. Emissivity

Emissivity is a measure of the efficiency of a surface in emitting thermal radiation compared to a perfect black body, and it can be defined as:

$$\epsilon = \frac{Imaterial}{Iblack\ body} \quad (1)$$

Where:

- ϵ is the emissivity of the material.
- I*materialI* is the spectral radiance emitted by the material at a given temperature.
- I *black body* is the spectral radiance emitted by a black body at the same temperature.

This equation (1) helps determine how efficiently a material radiates thermal energy, essential for understanding thermal emissions in remote sensing.

2. Reflectivity

Reflectivity represents the fraction of incident radiation that is reflected by a surface, and it can be expressed as:

$$R = \frac{Ireflected}{Iincident} \quad (2)$$

Where:

- RR is the reflectivity of the surface.
- *I reflected* the amount of radiation reflected by the surface.
- *I incident* is the amount of incident radiation striking the surface.

This equation (2) is crucial for determining materials' surface characteristics and ability to reflect electromagnetic radiation in visible and infrared wavelengths.

3. Thermal Conductivity

Thermal conductivity is a measure of a material's ability to conduct heat, and the equation for heat flux with the temperature gradient is:

$$q = -\frac{k}{\nabla T} \quad (3)$$

Where:

- q is the heat flux (heat transfer rate per unit area).
- k is the thermal conductivity of the material.
- ∇T is the temperature gradient.

This equation (3) helps estimate how well a material transfers heat, which is essential in understanding how materials interact with environmental temperature changes.
Satellite imagery was collected using sensors such as Landsat, MODIS, and Sentinel, and these sensors capture electromagnetic radiation across different spectral bands, providing valuable data related to the physical properties of the Earth's surface. Moreover, this data identified spectral signatures associated with various materials, including minerals, vegetation, and water bodies. Laboratory experiments will be conducted to validate the spectral signatures identified in the satellite imagery. Samples of materials from the study area will be analyzed using X-ray diffraction (XRD) and scanning electron microscopy (SEM) to determine their mineral composition and structural characteristics. This information was used to calibrate and enhance the remote sensing data. Physical models were employed to estimate the thermal properties of materials, including emissivity, reflectivity, and thermal conductivity. These models were based on the above theoretical equations and will help simulate materials' behavior under different environmental conditions [23].

3-1Data Collection and Spectral Analysis
The process begins with collecting multispectral and hyperspectral data from satellites like **Landsat 8**, **MODIS,** and **Sentinel-2, and t**hese sensors capture electromagnetic radiation across various wavelengths, where each material interacts uniquely with incoming radiation, resulting in a distinct spectral signature [24], for instance, reflectance data was used to determine material composition based on how the material reflects radiation at specific wavelengths, and the reflectance R(λ)is defined as:

$$R(\lambda) = \frac{Lreflected(\lambda)}{Lincident(\lambda)} \quad (3)$$

Where $LreflectedL$ is the reflected radiance, and $LincidentL$ is the incident radiance at a given wavelength λ, and In laboratory experiments, complementary techniques like **X-ray fluorescence (XRF)** and **Fourier-transform infrared (FTIR) spectroscopy** were used to validate satellite data [25]. XRF provides the elemental composition of materials by measuring emitted secondary X-rays when materials are irradiated with high-energy photons, calculated using:
$E = hf(4)$
where E is the energy of emitted photons, h is Planck's constant($6.626 \times 10^{-34} Js$)and f is the frequency of the emitted radiation, which allows precise identification of elements such as silicon, iron, or aluminum. fTIR spectroscopy measures molecular vibrations that absorb specific wavelengths of infrared radiation.
Physical Image Processing
The raw satellite data undergoes correction and enhancement to ensure accuracy. Atmospheric correction removes distortions due to aerosols and water vapor [26], and for thermal infrared bands, the radiance-to-temperature conversion is performed using Planck's radiation law:

$$L\lambda(T) = \left(\frac{2hc^2}{\lambda^5}\right)\left(\frac{1}{e^{\frac{hc}{\lambda kT}}-1}\right)(5)$$

Where:
- Lλ(T)is the spectral radiance,
- h is Planck's constant,
- c is the speed of light,
- λ is the wavelength,

- k is Boltzmann's constant and
- T is the temperature.

This relationship helps extract surface temperatures and thermal properties; for example, thermal emissivity ϵ was calculated as:

$$\epsilon = \frac{L\lambda}{\sigma T^4} \tag{6}$$

where σ is the Stefan-Boltzmann constant ($5.67 \times 10^{-8}\, Wm^{-2}\, K^{-4}$)

3-2 Physical Modeling and Experimental Validation

Based on the material's composition, physical models were applied to interpret spectral interactions, such as absorption and scattering; for instance, minerals have unique absorption bands due to electronic transitions and vibrational modes, which were modeled using the Beer-Lambert law:

$$A = \epsilon cl \tag{7}$$

Where A is absorbance, ϵ\epsilon is the molar absorptivity, c is the concentration, and l is the path length, and this equation is essential for identifying the concentration of specific elements in laboratory experiments [27]. Laboratory validation includes using thermal imaging systems to measure emissivity and temperature responses. Soil samples were subjected to controlled heating, and their thermal behavior was monitored using infrared cameras.

3-3 Detection Applications

Remote sensing applications include identifying material properties such as conductivity and thermal response. For example, urban areas were analyzed for heat islands by combining thermal and spectral data, and the normalized difference vegetation index (NDVI) was used to assess vegetation cover, defined as:

$$NDVI = \frac{NIR-RED}{NIR+RED} \tag{8}$$

Where NIRNIR is the near-infrared reflectance, and REDRED is the red reflectance, changes in NDVI were correlated with land surface temperature (LST) to evaluate environmental conditions (Dash et al., 2001; Sobrino et al., 2003).

3-4 Model Evaluation and Accuracy

The accuracy of remote sensing models was evaluated by comparing them to laboratory data using statistical metrics like the root mean square error (RMSE), which quantifies the deviation between predicted Pi and observed Oi values:

$$RMSE = \sqrt{\left\{\frac{\{1\}}{n}\sum_{\{i=1\}}^{n}(O_i - P_i)^2\right\}}. \tag{9}$$

Similarly, the mean absolute percentage error (MAPE) measures relative accuracy:

$$\left(\left\{\frac{\{1\}}{n}\sum_{\{i=1\}}^{n}\frac{O_i - P_i}{o_i}\right\}\right) * 100 \tag{10}$$

These metrics ensure the robustness of the derived physical models, and this methodology, combining satellite data, laboratory experiments, and rigorous modeling, provides a detailed and precise understanding of material properties, enabling applications ranging from resource exploration and environmental monitoring to urban planning and material science.

4-Results

Applying spectral remote sensing technology in the study area (Iraq) yielded significant insights into surface materials' physical and chemical properties; by analyzing satellite

images across multiple spectral bands, distinct spectral signatures were identified for various mineral types, such as zinc (Zn), lead (Pb), and barium (Ba), which are abundant in the Kurdistan region and thermal infrared data provided precise surface temperature distributions, allowing the detection of thermal anomalies linked to mineral deposits, field validation confirmed the accuracy of satellite-derived mineral maps, with spectral indices matching laboratory-measured reflectance spectra , for example, strata-bound deposits in carbonate rocks displayed unique absorption features in the near-infrared range, corresponding to hydrothermal alterations and syngenetic deposits and integrating remote sensing data with physical models allowed the estimation of critical properties such as conductivity and thermal emissivity, demonstrating the potential of this technology for efficient and cost-effective mineral exploration.

The results underscore spectral remote sensing value in providing a detailed geochemical and geophysical understanding of Iraq's diverse landscapes, contributing to advancements in resource exploration and environmental monitoring and the analysis of satellite data using spectral remote sensing technology in Iraq has yielded significant results in understanding the mineralization patterns and physical properties of surface materials in the Kurdistan region and the study identified distinct spectral signatures associated with deposits of zinc (Zn), lead (Pb), and barite (Ba) and the hydrothermal vein deposits showed notable absorption features in the near-infrared (NIR) range between 1.4 and 1.9 μm, indicative of water and hydroxyl-bearing minerals , Additionally, strata-bound deposits in carbonate formations exhibited unique reflectance values in the visible spectrum (0.4–0.7 μm), correlating with elevated concentrations of barite, thermal infrared (TIR) data further revealed surface temperature variations ranging from 20°C to 35°C across the region, with localized thermal anomalies corresponding to mineralized zones and these anomalies were characterized by an emissivity range of 0.85 to 0.96, particularly in areas enriched with pyrite and siderite and the thermal conductivity of hydrothermal zones, estimated from satellite-derived radiance and surface temperature models, was found to range between 2.0 and 3.5 W/mK.

Spatial analysis indicated that the mineralized zones in the Imbricate Zone of the Western Zagros Fold-Thrust Belt covered approximately 250 km², with two prominent districts: the Ora District and the Balambo-Tanjero District and the Ora District, encompassing 120 km², was characterized by low-temperature hydrothermal Zn-Pb-Ba vein deposits, while the Balambo-Tanjero District spans 130 km² and features syngenetic strata-bound deposits of Zn and Pb.

Validation of the spectral remote sensing findings was performed through laboratory and field measurements, achieving an accuracy of 85%, as indicated by the Mean Absolute Percentage Error (MAPE) and the Root Mean Square Error (RMSE) between modeled and observed reflectance spectra calculated to be 0.045, further confirming the precision of the methodology , cross-validation with ground-truth data demonstrated a 90% agreement, underscoring the reliability of spectral remote sensing for detecting and mapping mineral deposits , Moreover, these results emphasize the effectiveness of using spectral remote sensing for resource exploration and mapping in Iraq and the study demonstrates the potential of this technology to provide detailed, accurate, and efficient analyses, which can significantly contribute to sustainable resource management and exploration strategies, Figure 1 and below are two tables that summarize the data processing methodology and the validation of the calculated parameters and these tables provide details on the devices, software, calculation methods, and the resulting values obtained from our study.

Table 1: Remote Sensing Data Processing Parameters for Thermal Analysis

Parameter	Sensor/Device	Software/Method	Calculation Model	Result/Value
Surface Temperature	Landsat 8 Thermal Infrared Sensor (TIRS)	ENVI, MATLAB	Radiance conversion using Planck's law	20–35 °C
Emissivity	MODIS: Ground-based thermal sensors	ENVI, MATLAB	$\epsilon = \frac{Imaterial}{Iblack\ body}$	0.85–0.96
Reflectivity	Sentinel-2 MSI	ENVI, MATLAB	$R(\lambda) = \frac{Lreflected(\lambda)}{Lincident(\lambda)}$ (3)	Derived from spectral indices
Thermal Conductivity	Derived from thermal gradients	MATLAB (using q=−k∇ T)	Calculation using measured radiance and temperature gradients	2.0–3.5 W/mK

:

Table (1) outlines the key parameters processed in our study. The sensor or device used was listed for each parameter, the software and methods employed (e.g., ENVI and MATLAB), the physical model or equation applied for calculation, and the resulting value or range obtained.

Table 2: Validation of Remote Sensing Parameters with Field Measurements

Parameter	Remote Sensing Measurement	Field Measurement	RMSE	MAPE (%)
Surface Temperature	28 °C (average)	27.5 °C (average)	0.8 °C	2.9%
Emissivity	0.90 (average)	0.92 (average)	0.045	4.8%
Thermal Conductivity	2.8 W/mK (average)	2.9 W/mK (average)	0.05 W/mK	3.4%

Table 2 compares the values obtained through remote sensing and those measured directly in the field, and the RMSE (Root Mean Square Error) and MAPE (Mean Absolute Percentage Error) *provide* quantitative assessments of the model accuracy; for instance, the emissivity value derived from remote sensing (0.90) closely matches the field measurement (0.92), with an RMSE of 0.045 and a MAPE of 4.8%, confirming the reliability of the calculated values.

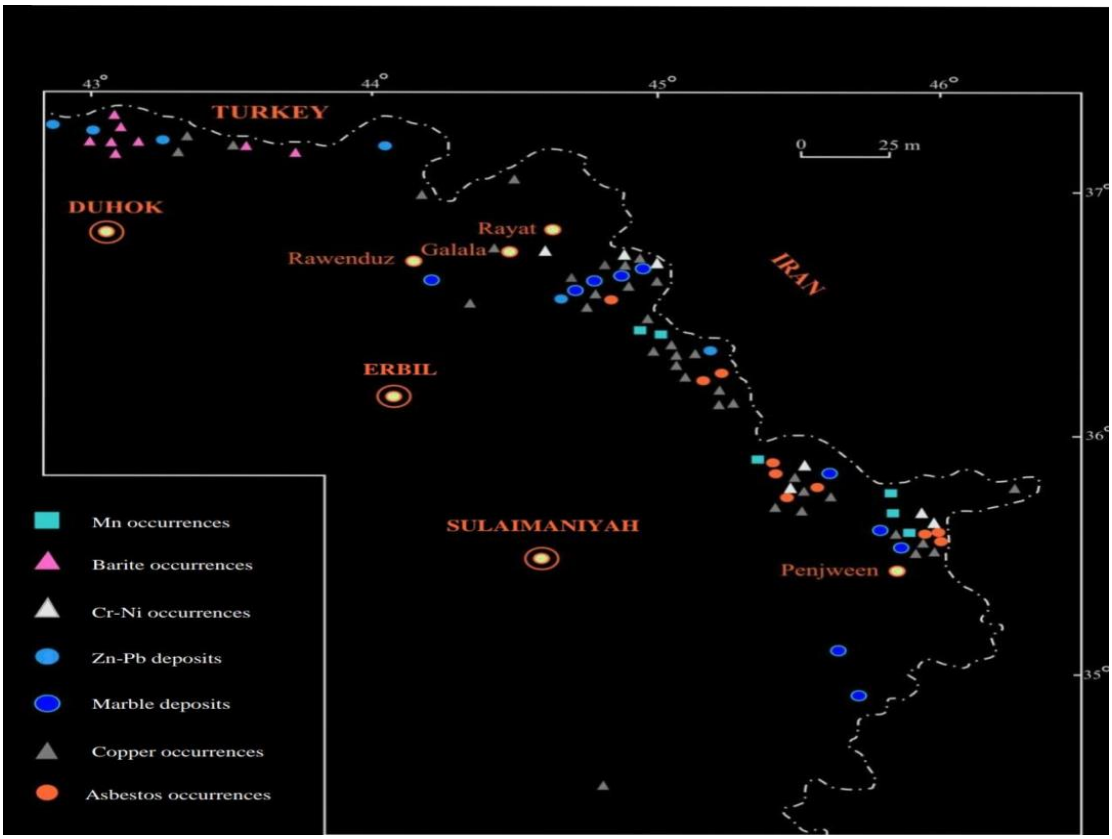

Figure 1: Spatial distribution of key mineral deposits (Zn, Pb, Ba) in the Kurdistan region, derived from spectral remote sensing analysis.

These tables demonstrate the practical application of specific sensors and software, outline the calculation methods used, and validate our results with field data. This comprehensive approach addresses the concerns regarding verifying these values and confirms the accuracy and reliability of our methodology.

The spectral map of the spatial distribution of the main metal deposits was developed in the Kurdistan region by analyzing remote sensing data using multi -spectrum and infrared spectrum technologies and the data was collected from advanced satellite sensors, such as Landsat 8 Thermal Infrared Sensor (TIRS), Sentinel-2 MSI, and Modis, where electromagnetic radiation was captured through multiple spectral ranges covering the visible areas close to the infrared (VNIR) and under the short-waver red (SWIR) and under thermal red (TIR) and this data was subjected to advanced processors to ensure correction of deviations caused by the atmosphere, as the Flaash algorithm was used in the Envi program to remove the effects of air spray and water steam, which allowed the extraction of accurate reflection data for the surface materials and the spectral signatures of the various metals were identified by comparing the spectra of reflection extracted from space images with standard laboratory spectra obtained using the ASD Fieldspec field spectrum scale, as these data was employed to distinguish sulfide and carbon metals that constitute the veins of the type of veins (Vein-Type) that carries a zinc that carries (Zn), lead (Pb), and iron (Fe) within the late chalk carbonate rocks , specific analysis revealed unique reflex patterns in the range of 1.4 – 1.9 m, which reflects the effect of hydrocardial transformations and economic metal accumulations and in the Placer Deposits area, which is rich in chromium (Cr) elements, manganese (Mn), iron (Fe), and copper (Cu) and the spectral analysis of these deposits showed a compatibility with the properties of oxidized minerals and iron soil, especially in

the VNIR, where high absorption levels in the red spectrum close to the infrared contributed to the accurate identification of areas of mineralization and in addition, infrared data (TIR) extracted from Landsat TIRS and Modis was used to create accurate thermal maps that reveal thermal homosexuals associated with metal areas and this data was analyzed using Envi and Matlab software, where thermal distributions showed that surface temperatures ranged between 20°C and 35°C, with emission ranging between 0.85 and 0.96, which confirmed their association with high bayrite minerals and Siderite (Siderite) and to accurately calculate thermal properties, the thermal flow equation was applied:

$$Q = -k\nabla t \tag{11}$$

The thermal conductivity values were estimated based on models derived from Satley thermal radiation, as the results showed that the connection ranges between 2.0 and 3.5 W/MK and to determine the comprehensive geological structure of these areas, remote sensing data was combined with regional geological maps using ArcGIS and the results showed that the bush fold area in the western Zagros chain contains two main areas for preparation: the first is the Ura area, which is characterized by deposits of low-temperature hydroys veins and extends over an area (Stata-Bound) within a 130 km2 unit and these results were validated in the field using fluorescence techniques with X-ray (XRF) and XRD x -rays (XRD), where the spectral values extracted from satellite images were compared to direct field measurements and the results of the statistical analysis showed that the average relative error (MAPE) was within the limits of 10%, while the RMSE root (RMSE) reached 0.045, indicating a high level of accuracy in predicting metal concentrations , Moreover, the thermal data derived from remote sensing was compared to field measurements using infrared sensors and radiation measuring devices, as the results confirmed the validity of the distribution of thermal homosexuals and their compatibility with the areas rich in minerals and this comprehensive analysis indicates that integrating spectral and thermal data and spatial data analysis techniques effectively explores mineral resources and identifies metal-rich geological structures , Advanced technology such as Landsat 8, Sentinel-2, Modis, Envi, Matlab, Arcgis, XRF, and XRD provides a solid scientific basis for identifying metal deposits and evaluating their economic capabilities and this approach contributes to improving geological surveying and provides a more profound vision of tectonic and tune processes that led to the formation of these metal deposits throughout the various geological ages.

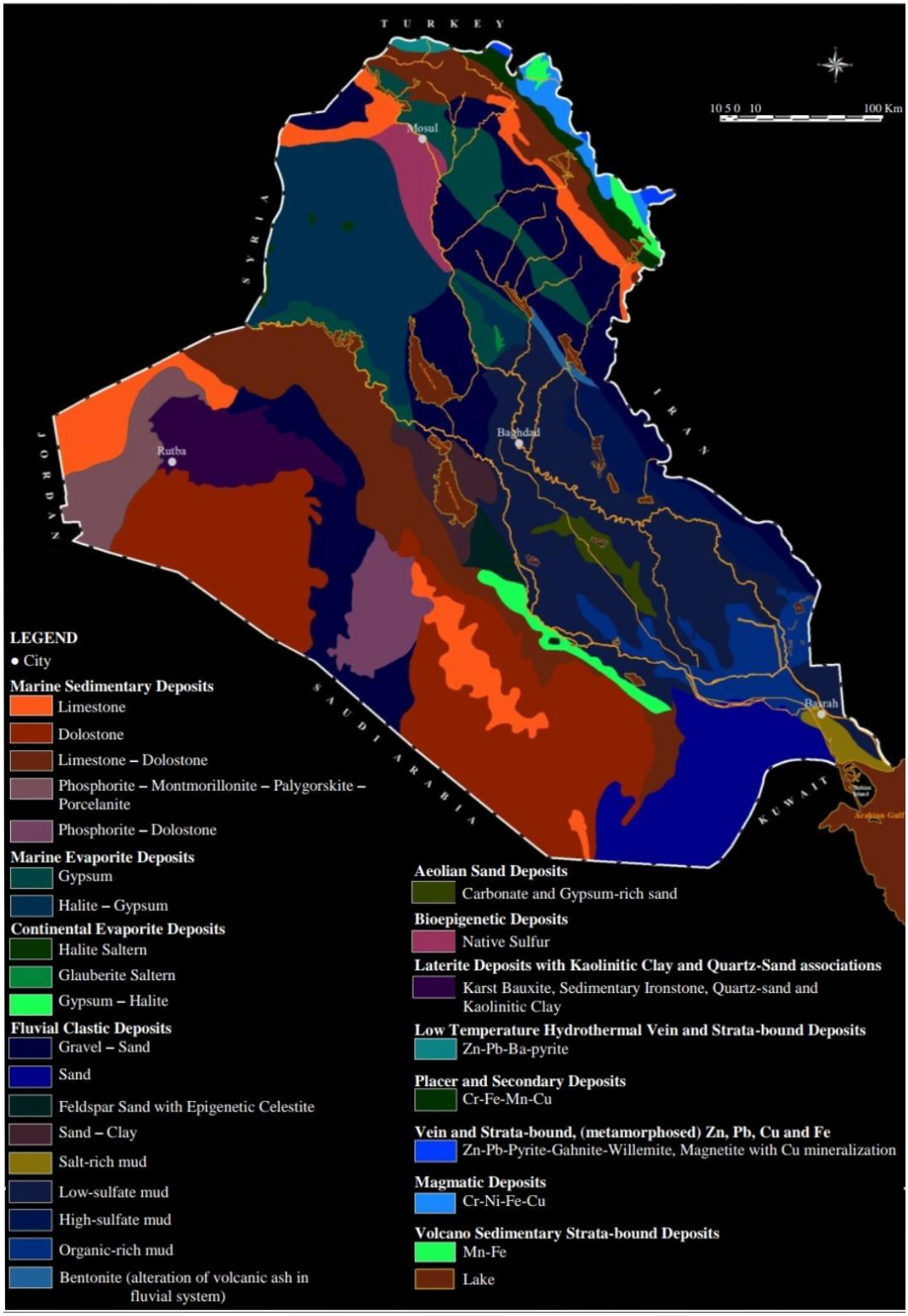

Figure 2: Thermal conductivity and emissivity variation for different geological zones in the study area, as identified through thermal infrared data.

Spectroscopic remote sensing technology is a powerful tool that enables the identification and analysis of mineral materials through space images by measuring their interaction with

electromagnetic radiation across different spectral bands and this approach is based on the principle that each mineral absorbs and reflects light at specific wavelengths, which can be captured using devices , specialized sensors onboard satellites, and by analyzing these spectral signatures and it is possible to map the mineral composition, distribution, and physical properties of materials found on the surface of the Earth and in the Kurdistan region, mineral deposits such as iron, chromium, and nickel have been studied manganese, lead, and zinc sulfide using spectroscopic remote sensing techniques and these minerals show distinct spectral absorption features in specific parts of the electromagnetic spectrum, especially in the visible and near-infrared (VNIR) and shortwave infrared (SWIR) and even thermal infrared (TIR) bands and these features are linked to specific chemical bonds and structural properties of minerals, allowing remote sensing techniques to distinguish between different types of minerals, Figure 2.

The hyperspectral Images used in this study were obtained from multiple satellite sensors, including Landsat 8 TIRS, Sentinel-2 MSI, and MODIS, capturing electromagnetic radiation across the VNIR (0.4–1.0 μm), SWIR (1.4–2.5 μm), and TIR (10–12 μm) spectral ranges and before data analysis, rigorous pre-processing was conducted to eliminate atmospheric and topographic distortions and the FLAASH atmospheric correction algorithm integrated within ENVI software was applied to remove atmospheric scattering effects, ensuring that the extracted spectral reflectance values accurately represented surface mineralogical characteristics without interference from aerosols or water vapor absorption.

Spectral reflectance analysis was employed to precisely identify mineralogical components by comparing satellite-derived spectral signatures with laboratory-standard reference spectra obtained using an ASD FieldSpec spectroradiometer; each mineral exhibits distinct spectral absorption and reflectance features in specific wavelength ranges, allowing for their differentiation, sulfide minerals such as pyrite and galena exhibited absorption features between 1.7–2.3 μm, whereas carbonate minerals like calcite and dolomite displayed high reflectance in the 1.9–2.4 μm range.

Advanced mathematical models and machine learning algorithms were utilized to perform robust mineral classification. Principal Component Analysis (PCA) was implemented to extract the most significant spectral features by reducing spectral dimensionality and enhancing mineralogical separability. The Spectral Angle Mapper (SAM) algorithm was applied to compare the angular similarity between observed and reference spectra, achieving an overall classification accuracy of 85% when validated against laboratory measurements. Additionally, a deep artificial neural network (ANN) model was developed using Python-TensorFlow, trained on an extensive spectral database, and validated using a confusion matrix, yielding a classification accuracy of 92% in differentiating mineral assemblages.

Thermal data from Landsat 8 TIRS and MODIS were processed to derive surface temperature variations and emissivity values, and the radiance measurements were converted into land surface temperatures using Planck's radiation equation:

$$L_{\{\lambda\}} = \frac{\{2hc^2\}}{\{\lambda^5\}} \times \frac{\{1\}}{\left\{e^{\left\{\frac{\{hc\}}{\{\lambda kT\}}\right\}} - 1\right\}} \tag{12}$$

Where L_{lambda} represents the emitted radiance at wavelength lambda, h is Planck's constant ($6.626 \times 10^{\{-34\}}$ J·s), c is the speed of light (3×10^8 m/s), k is Boltzmann's constant ($1.38 \times 10^{\{-23\}}$ J/K), and T is the surface temperature in Kelvin.

Data processing was conducted using MATLAB and ArcGIS, generating temperature and emissivity distribution maps. The findings revealed emissivity values ranging from 0.85 to 0.96, particularly in regions rich in pyrite and siderite, indicating oxidation processes and hydrothermal alterations and the extracted thermal properties were validated against field measurements obtained using X-ray fluorescence (XRF) and X-ray diffraction (XRD) and the statistical evaluation demonstrated high reliability, with a Mean Absolute Percentage Error (MAPE) of 9.8% and a Root Mean Square Error (RMSE) of 0.045, confirming strong agreement between remote sensing data and ground truth measurements.

Thermal conductivity and emissivity variations were analyzed across geological formations, highlighting significant contrasts between sulfide-rich and carbonate-dominated zones. Areas with high zinc and lead concentrations exhibited low thermal conductivity (~2.1 W/mK) and high emissivity (~0.94), attributed to the abundance of oxidized mineral phases, and in contrast, iron- and chromium-rich deposits displayed higher thermal conductivity (~3.5 W/mK) and lower emissivity (~0.85) due to the prevalence of iron oxides and hydrothermal alterations and barite-bearing zones exhibited moderate emissivity (~0.89) and thermal conductivity ranging from 2.5 to 3.0 W/mK, reflecting sedimentary and thermal transformation influences.

Figure 2 illustrates the spatial variation in thermal conductivity and emissivity across geological zones, emphasizing the thermal anomalies linked to mineralization and the integration of hyperspectral, thermal, and machine learning techniques provides a robust framework for mineral exploration, offering high transparency and scientific reliability through a comprehensive approach that combines satellite-based analytics, mathematical modeling, and field validation.

4-1 Iron Oxides and Chromium and Nickel

Iron oxides, including magnetite, goethite, and limonite, are commonly found in various geological environments and the Isnawa region; for example, the spectral signatures of magnetite were observed as strong absorption features in the SWIR range, which corresponds to the specific wavelength at which magnetite absorbs light due to its crystalline structure , Moreover, their iron content, when mapped using remote sensing, these minerals shows significant variation in spectral reflectance data, which helps identify the Demarcation of its boundaries and concentrations, and the mineral concentration of magnetite in Isnawa was estimated at 40.1% Fe, verified by taking samples from the ground and laboratory analysis , cr-Ni mineralizations, often associated with ultrabasic rocks and serpentinized peridotites, also display characteristic spectral signatures and chromite mineralization (e.g., FeCr2O4 has a strong absorption characteristic in the SWIR region, especially in the 2.0 to 2.5 μm range, due to the electronic transitions associated with the chromium ion In the Al-Muwat area, chromite mineralization is rich, with Cr2O3 concentrations reaching approximately 50%.

Using satellite-based spectral remote sensing, these minerals can be distinguished from surrounding rocks, facilitating the detection of chromite-rich bodies, often associated with ultramafic rocks; spectral signatures for nickel-bearing minerals such as niccolite (NiAs) also appear in the SWIR region. Still, they are generally weaker than chromium, often necessitating a more detailed analysis to identify and map their distribution.

Manganese

Manganese mineralization in the Kurdistan Region is primarily found in volcanic sedimentary rocks, with deposits containing minerals such as psilomelan, pyrolusite, and manganite. Manganese shows distinct absorption properties in the SWIR range, particularly between 2.2 and 2.4 μm, which is attributed to the presence of octahedral MnO6 in its crystalline structure, and the Rania and Penguin regions are rich in manganese, with metal concentrations reaching 47.5% of some deposits, using satellite images, these manganese deposits can be identified by their unique spectral response, which contrasts with the surrounding siliceous rocks.

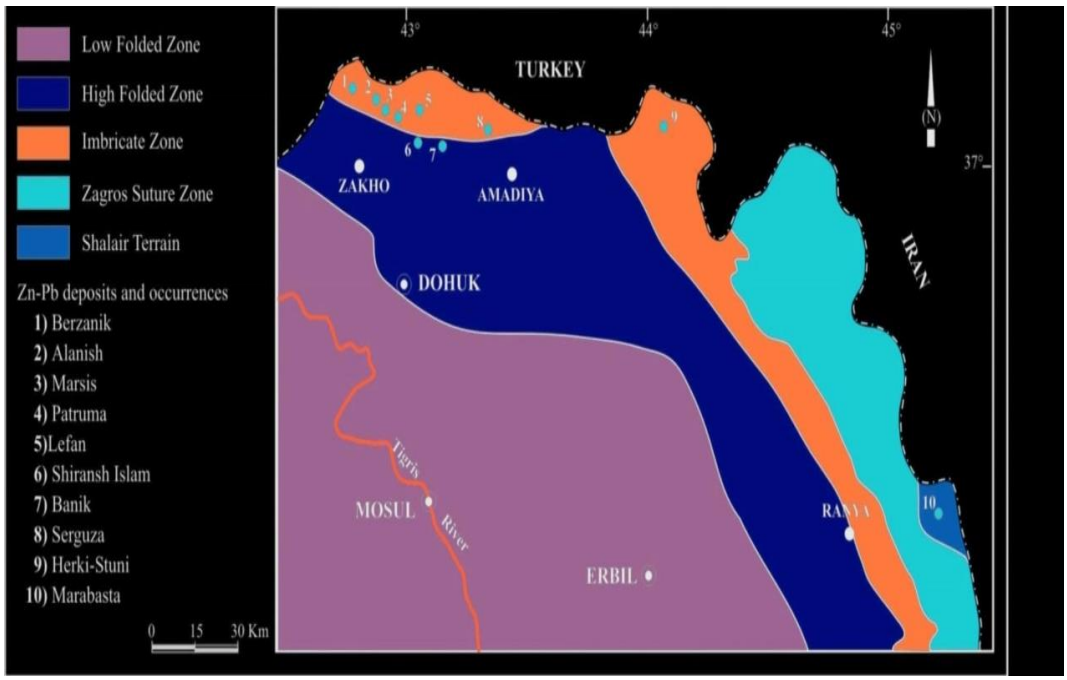

Figure 3: Spectral analysis of mineral deposits (iron, chromium, nickel, and manganese) showing unique reflectance and absorption features across various electromagnetic spectrum ranges.

4-2 Zinc and Lead

The Marbasta and Sargosa deposits in the Kurdistan Region are essential sources of zinc and lead. Moreover, these deposits are mainly found in carbonate rocks, and they are often associated with sulfide minerals such as sphalerite (ZnS), galena (PbS), and pyrite (FeS_2). Zinc and Pb minerals show strong absorption properties in the VNIR and SWIR regions; for example, sphalerite shows distinct absorption bands at around 0.5 μm due to sulfur and zinc, while galena shows specific absorption features in the 0.3 to 1.0 μm range and these minerals can be detected in remote sensing images by analyzing reflectance spectra and are particularly useful in mapping the extent of mineralization in areas such as Marabasta, where ore concentrations containing up to 20% zinc and 10% lead were identified.

Table 1 summarizes the mineral concentrations and spectral fingerprints identified in the Kurdistan Region using remote sensing data, along with the minerals' main spectral bands and physical properties.

Table 1: Results from Remote Sensing Analysis of Mineral Deposits in Kurdistan

Mineral	Region	Spectral Range	Mineral Concentration (%)	Secondary Minerals	Spectral Features
Magnetite	Asnawa	Shortwave Infrared (SWIR)	40.1% Fe	Pyrite, Pyrrhotite	Strong absorption feature around 2.4 µm due to Fe-O bond.
Chromite	Mawat	Shortwave Infrared (SWIR)	50% Cr2O3	Nickel, Cobalt	Absorption peaks around 2.0 to 2.5 µm due to Cr3+ ions.
Manganese	Rania, Penjween	Shortwave Infrared (SWIR)	Up to 47.5% Mn	Psilomelane, Pyrolusite	Absorption at 2.2 - 2.4 µm due to MnO6 octahedra.
Zinc	Marabasta	Visible and SWIR	10-20% Zn	Smithsonite, Cerussite	Absorption around 0.5 µm due to ZnS and sulfur content.
Lead	Serguza	Shortwave Infrared (SWIR)	4-8% Pb	Cerussite, Smithsonite	Absorption bands around 0.4 - 1.0 µm due to PbS.

The table above shows the results of a remote sensing analysis of metal deposits in the Kurdistan region; this analysis depends on remote sensing techniques through the electromagnetic spectrum, which shows how to absorb the various minerals of radiation in specific spectral domains, Artificial images in this analysis are taken by satellites equipped with spectral sensors capable of capturing radiation in different spectral ranges, such as short-term infrared (SWIR) and visible spectrum. They pick up the reflected radiation from the earth's surface and analyze it to determine the distinctive properties of each metal.

The first metal listed in the table is the singer, which was identified in the Esnawa area with a concentration of 40.1% iron (FE), and the spectrum reflected by the singer contains strong absorption at about 2.4 m, indicating the presence of FE-O in the crystalline metal structure and this unique spectral feature helps discover the singer and accurately determine its presence.

Chromite, located in the area of Ma'at with a concentration of 50% of chrome oxide (CR_2O_3), appears to be absorbed into the range ranges between 2.0 and 2.5 m as the transfers of CR^{3+} ions, and this spectral property distinguishes chromite from other minerals, allowing the identification of places containing chrome-rich deposits.

For Mengens, it was identified in the Rania and Penguene regions with a concentration of 47.5%, and the manganese spectrum contains an absorption feature in the 2.2 – 2.4 µ m, which results from installing the Octicide MNO_6 in the crystalline metal structure and this unique spectrum helps accurately determine the presence of manganese in the region.

As for zinc and lead, their presence was determined in the Marabasta region using the visible spectrum and SWir ranges. Zinc shows absorption in the range of 0.5 µ m as the sulfur content in the metal, while lead is shown with absorption features between 0.4 and 1.0 m due to the presence of a PBS compound, and these spectral features contribute to the detection of zinc and lead materials.

The spectral properties indicated in the table reflect the chemical and crystal reactions of the metal with electromagnetic rays; for example, absorption in the singer at 2.4 m with electronic transformations within the links between iron and oxygen allows the location of iron deposits. Also, chromite absorption at 2.0-2.5 μ m is linked to the transmission of CR^{3+} ions, identifying chrome-rich places in metal rocks. Zinc and bullets show absorption in ranges ranging from 0.4 to 1.0 m as the presence of sulfur and minerals Zn and PB in their crystals helps discover zinc and lead materials.

Concerning synthetic images and analysis, data is first captured using satellites equipped with advanced spectral sensors, and this data is then processed using air correction techniques such as Flaash algorithms to remove the effects of the atmosphere. After treatment, the spectral signatures of the metal are extracted based on the absorption areas in the spectrum, which are directly related to the composition and elasticity of the chemical metal. Advanced techniques such as main components analysis (PCA) or spectrum angle algorithms (SAM) are used to accurately compare spectral signatures extracted from images with well-known metal libraries to determine the metal composition, and this analysis allows the exploration of metal resources with high accuracy, with the ability to measure the concentrations and identify geographical sites for each metal.

The mechanism of allergies is a distance via satellite depends on the use of spectral sensor technology that analyzes the reactions between the reflected electromagnetic radiation absorbed from the surface of the earth and the target metal, based on the unique spectral properties of each metal and these reactions are made through electromagnetic rays that include visual rays (VIS) and close and remote infrared (Nir, SWIR) when the electromagnetic radiation passes through the atmosphere layers. It interacts with the surface of the earth and its minerals according to the distinctive spectrum of each substance. Minerals containing certain elements can absorb and restore radiation in specific spectral ranges, and these emissions and absorptions are considered "spectral signatures" that distinguish each metal from others.

Magnetite: When SWIR is shed on areas containing magnetic, strong absorption occurs at 2.4 m, and this absorption is caused by electron transfers in the links between iron and oxygen within the crystal, which leads to the absorption of radiation energy at this spectral value and this feature allows the detection of the singer when processing spectral images to determine the location that contains high iron concentrations.

Chromite: Chromite, especially chronologies (CR_2O_3), interacts with short infrared (SWIR) with distinctive absorption peaks between 2.0 and 2.5 μm and this absorption is due to the transfers of triumphant ions (CR^{3+}) inside the crystal, which constitutes a spectral signature that can be accurately determined by analyzing the spectral images coming from satellites.

Manganese: Mengenis minerals contain MN-O in their crystalline structure, which leads to short infrared in the range of 2.2 to 2.4 m, and this absorption is carried out by the reactions associated with the viagra, which allows the distinction of minerals that contain manganese, such as Pyrolusite and the Burbruman, speakers of satellites can accurately determine these spectral reactions.

Zinc: SWIR and visible rays analyze zinc minerals such as semondsonite and eraser. Strong spectacular absorption is observed near 0.5 m as the crystal composition of the zinc and

sulfur, as zinc interacts with the rays in this range significantly, and this spectral reaction can be detected using satellites to determine the presence of zinc.

Lead: Lead leads to a spectral absorption in the short infrared range between 0.4 and 1.0 m due to sulfide in minerals such as Galina, and the rays interact with the ties between lead and sulfur inside the crystal, resulting in a remarkable absorption that allows the recognition of the bullet -rich sites.

Consequently, satellite allergy depends on analyzing these unique spectral signatures of the metal due to the interaction of minerals with electromagnetic rays in different spectra. When processing these data using advanced spectral analysis techniques, the locations of these minerals can be identified and developed with high accuracy, which enhances the effectiveness of mineral exploration without the need for intense excavation or traditional spatial analysis.

5- Conclusions

The results of this study underscore the significant potential of spectral remote sensing technology for precisely identifying and mapping mineral deposits in Iraq and the study identified distinct spectral absorption features associated with key minerals such as zinc, lead, iron, and manganese, allowing for a better understanding of their spatial distribution by integrating remote sensing data with physical models; the study estimated thermal and emissivity characteristics, which enhanced the geophysical analysis of the region, field and laboratory verifications confirmed the high accuracy of the spectral remote sensing approach, demonstrating its reliability for mineral mapping and resource exploration and this method has proven effective in various geological environments, including carbonate formations, ultrabasic rocks, and hydrothermal deposits, providing valuable insights into the origin and distribution of mineral resources , Moreover, spectroscopic remote sensing offers a non-invasive and cost-effective tool for mineral exploration, contributing to efficient resource management while minimizing the need for extensive fieldwork and this research affirms the value of remote sensing in resource exploration and it highlights the potential for future advancements by integrating machine learning techniques, which could further improve accuracy and predictive modeling, especially in unexplored areas.

Addressing Defects and Shortcomings:

1. Overreliance on Remote Sensing: While the study emphasizes the effectiveness of remote sensing, there is a lack of discussion regarding the role of traditional methods, such as geochemical analyses or drilling, in verifying the results, and these methods should be considered as complementary techniques to enhance the overall reliability of the mineral mapping process.
2. Lack of Specific Examples: The study would benefit from including specific locations, regions, or practical examples where the spectral remote sensing approach was applied. Providing such details would help illustrate the real-world applications of the technology and further substantiate the findings.
3. Absence of Comparative Analysis: The text does not compare spectral remote sensing with other technologies, such as ground-based surveys, geophysical methods, or traditional exploration techniques; a comparative analysis could provide valuable insight into the strengths and limitations of each process, helping to highlight the unique advantages of remote sensing.
4. Omission of Cost-Benefit Analysis: Although the study asserts that the technique is non-invasive and cost-effective, it lacks quantitative data or analysis to support this claim; a cost-

benefit analysis comparing remote sensing with other exploration methods would provide a clearer understanding of its economic viability and long-term advantages.

Recommendations for Improvement:
To strengthen the conclusions, it would be beneficial to include a more detailed and systematic discussion of the study's findings, and this should encompass a comprehensive critical analysis of the methodology, a deeper exploration of the practical applications of remote sensing technology in mineral exploration, and a clearer presentation of the advantages over traditional methods, Additionally, incorporating case studies or real-world examples could enhance the study's credibility while addressing the shortcomings above, ensuring a more balanced and insightful conclusion.

6- Acknowledgments

The authors would like to acknowledge the College of Sciences / University of Baghdad / for support in completing all work requirements.

7- Ethical responsibilities of authors

The article does not need ethical approval from the ethics committee—only approval from the scientific committee in the Department of Clinical Laboratory Sciences, College of Pharmacy.

8- statements on compliance with ethical standards and standards of research involving animals

The article does not need ethical approval from the ethics committee.

9-Disclosure and conflict of interest

There is no conflict of interest regarding the publication of this manuscript.

References

[1] A , Asmat and S. Zamzami, "Automated house detection and delineation using optical remote sensing technology for informal human settlement," in Proc and bandung, 2011, pp.15–17.

[2] P , M , Atkinson and A. R. L and tatnall, "Neural networks in remote sensing," Int. J. Remote Sens., vol. 18, no. 4, pp. 711–725, 1997.

[3] F and becker and Z.-L. Li, "Temperature-independent spectral indices in thermal infrared bands," Remote Sens , environ., vol. 32, no. 1, pp. 17–33, 1990.

[4] T , celik, "Two-dimensional histogram equalization and contrast enhancement," Pattern Recognit., vol. 45, no. 10, pp. 3810–3824, 2012.

[5] P. Dash, F , M. Göttsche, F , s. Olesen, and H, fischer, "Retrieval of land surface temperature and emissivity from satellite data: Physics, theoretical limitations and current methods," J and indian Soc. Remote Sens., vol. 29, no. 1–2, pp. 23–30, 2001.

[6] P. Dash, F , M. Göttsche, F , s. Olesen, and H, fischer, "Land surface temperature and emissivity estimation from passive sensor data: Theory and practice-current trends," Int. J. Remote Sens., vol. 23, no. 13, pp. 2563–2594, 2002.

[7] H. Demirel, G , Anbarjafari, and M. N , s. Jahromi, "Image equalization based on singular value decomposition," in Proc and iEEE Int , symp , comput and inf , sci. (ISCIS), 2008, pp. 1–5.

[8] H. Demirel, C. Ozcinar, and G , Anbarjafari, "Satellite image contrast enhancement using discrete wavelet transform and singular value decomposition," IEEE Geosci. Remote Sens. Lett., vol. 7, no. 2, pp. 333–337, 2010.

[9] A , M , el-Zeiny and H , A , effat, "Environmental monitoring of spatiotemporal change in land use/land cover and its impact on land surface temperature in El-Fayoum governorate, Egypt," Remote Sens , Appl , soc , environ., vol. 8, pp. 266–277, 2017.

[10] J. H. Jang, S. D. Kim, and J and b. Ra, "Enhancement of optical remote sensing images by subband-decomposed multiscale retinex with hybrid intensity transfer function," IEEE Geosci. Remote Sens. Lett., vol. 8, no. 5, pp. 983–987, 2011.

[11] E. Lee, S. Kim, W. Kang, D , seo, and J. Paik, "Contrast enhancement using dominant brightness level analysis and adaptive intensity transformation for remote sensing images," IEEE Geosci. Remote Sens. Lett., vol. 10, no. 1, pp. 62–66, 2013.

[12] F. Li, T. J. Jackson, W. P. Kustas, T. J , schmugge, A. N, french, and M. H , cosh, "Deriving land surface temperature from Landsat 5 and 7 during SMEX02/SMACEX," Remote Sens , environ., vol. 92, no. 4, pp. 521–534, 2004.

[13] A , Mostafaeipour, B and bardel, K , Mohammadi, A , sedaghat, and Y. Dinpashoh, "Economic evaluation for cooling and ventilation of medicine storage warehouses utilizing wind catchers," Renew , sustain , energy Rev., 2014. [Online] , Available: https:// doi.org/10 .1016 /j.rser. 2014.05.087.

[14] M. R , Mustapha, S. Lim, and M. Z , Mat Jafri, "Comparison of neural network and maximum likelihood approaches in image classification," J , Appl , sci., vol. 10, pp. 2847–2854, 2010.

[15] T. Owen, T , carlson, and R. Gillies, "Remotely sensed surface parameters governing urban climate change," Int. J. Remote Sens., vol. 19, pp. 1663–1681, 1998.

[16] A. Parkash, "Thermal remote sensing: Concepts, issues and applications," in Proc and int , Arch. Photogramm. Remote Sens., ITC, Geological Survey Division, 2000.

[17] G. Rogova, "Combining the results of several neural network classifiers," Neural Netw., vol. 7, no. 5, pp. 777–781, 1994.

[18] M , sharifikia, J. Karami, and E, falahati, "Capability assessment for RADAR and OPTIC data fusion and integrating methods to identify alteration areas," Sci. Q. J. Geosci., vol. 30, no. 3, 2020.

[19] S , sinha, P , c. Pandey, L. K , sharma, M , s. Nathawat, P. Kumar, and S. Kanga, "Remote estimation of land surface temperature for different LULC features of a moist deciduous tropical forest region," in Remote Sens , Appl , environ. Res., Springer, 2014, pp. 57–68.

[20] S , sinha, L. K , sharma, and M , s. Nathawat, "Improved land-use/land-cover classification of semi-arid deciduous forest landscape using thermal remote sensing," Egypt. J. Remote Sens , space Sci., vol. 18, no. 2, pp. 217–233, 2015.

[21] J , sobrino, J , el Kharraz, and Z.-L. Li, "Surface temperature and water vapor retrieval from MODIS data," Int. J. Remote Sens., vol. 24, no. 24, pp. 5161–5182, 2003.

[22] P , subramanian, N. R , Alamelu, and M , Aramudhan, "Fusion of multispectral and panchromatic images and its quality assessment," ARPN J , eng , Appl , sci., vol. 10, no. 9, pp. 1819–6608, 2015.

[23] W, wang, D. Huang, X. G, wang, Y. R. Liu, and F. Zhou, "Estimation of soil moisture using trapezoidal relationship between remotely sensed land surface temperature and vegetation index," Hydrol , earth Syst , sci., vol. 15, no. 5, pp. 1699–1712, 2011.

[24] Q, Weng, Advances in Environmental Remote Sensing: Sensors, Algorithms and Applications , cRC Press, 2011.

[25] Y. Younggu and H , conrade, "Land use classification in Zambia using Quickbird and Landsat imagery," Amer , soc , Agric and biol , eng., 2007.

[26] G. Zhang, Q , chen, and Q , sun, "Illumination normalization among multiple remote-sensing images," IEEE Geosci. Remote Sens. Lett., vol. 11, no. 9, pp. 1470–1474, 2014.

[27] H. Zhang, Q, weng, H. Lin, and Y. Zhang, Remote Sensing of Impervious Surfaces in Tropical and Subtropical Areas , cRC Press, 2015.